Bottom-Up Construction of the Interaction Between Janus Particles

Alexander Popov[†] and Rigoberto Hernandez[*,†,‡,¶]

†*Department of Chemistry, Johns Hopkins University, Baltimore, Maryland 21218, USA*

‡*Department of Chemical & Biomolecular Engineering, Johns Hopkins University, Baltimore, Maryland 21218, USA*

¶*Department of Materials Science and Engineering, Johns Hopkins University, Baltimore, Maryland 21218, USA*

E-mail: r.hernandez@jhu.edu

Abstract

While the interaction between two uniformly charged spheres—viz colloids—is well-known, the interaction between non-uniformly charges spheres such as Janus particles is not. Specifically, the Derjaguin approximation relates the potential energy between two spherical particles with the interaction energy V_{pl} per unit area between two planar surfaces. The formalism has been extended to obtain a quadrature expression for the screened electrostatic interaction between Janus colloids with variable relative orientations. The interaction is decomposed into three zones in the parametric space, distinguished by their azimuthal symmetry. Different specific situations are examined to estimate the contributions of these zones to the total energy. The effective potential V_{pl} is renormalized such that the resulting potential energy is identical to the actual one for the most preferable relative orientations between the Janus particles. The potential energy as a function of the separation distance and the mutual orientation of

a pair of particles compares favorably between the analytical (but approximate) form and the rigorous point-wise computational model used earlier. Coarse-grained models of Janus particles can thus implement this potential model efficiently without loss of generality.

1 Introduction

Recent advances in mesoscale fabrication have allowed for the construction of anisotropic colloidal particles that are anticipated to self assemble into novel structure so as to unlock new material properties.[1–9] One example is the prediction of richer phase behavior for anisotropic colloidal materials[8,10–16] as can exist in gas, liquid, crystalline, or amorphous phases due to the order between particles in analogy with atomic materials. The Janus structure—wherein spherical particles have two chemically distinct hemispheres—is one such anisotropic colloid particle structure that has warranted much attention through experiment,[8,9,17–24] theory,[25–29] and simulation.[15,30–40]

Dipolar Janus (DJ) particles are a good target for materials development because they can be readily produced in large quantities. In one of the earliest attempts to prepare Janus particles, Veyssie et al[41] prepared them by protecting one hemisphere of glass spheres with a cellulose film while modifying the other hemisphere. Alternatively, Paunov and co-workers[42,43] used micro-contact printing technique to produce DJ colloids. In this technique, the particles are embedded onto an oppositely charged surface so as to protect the bottom hemispheres, and inoic surfactants are subsequently deposited on the top of the monolayer so as to coat to the top hemispheres. Meanwhile, Ikeda and co-workers[44,45] aggregate silica particles and modified only the accessible parts of the particles on a cluster surface. Granick el al[46] produce large quantities of Janus particles by partially trapping colloidal particles at the surface of even larger wax particles, thereby increasing dramatically the effective surface area of the embedded particles.

While the properties of DJ particle systems have been characterized experimentally to varying degrees, a full description of their properties has been greatly advanced through the use of computer simulation. One of the main challenges in describing the behavior of DJ particle systems in simulation is that their large size requires multi-scale characterization of their interaction. Indeed, the unsymmetrical nature of DJ particles makes it very difficult to accommodate a simple theoretical formula for the potential.

Hall et al[25,47] characterized the forces between the DJ colloids through a model consisting of hard spheres with two embedded point charges, focusing on the dipolar nature of the interaction. Though the dipolar term is the most important one,[30] the higher-order terms must also be considered.[19,21,24,29,48,49] Granick et al[17] emphasized that DJ colloidal particles are not well approximated by point dipoles as the size of the particles greatly exceeds the electrostatic screening length. Instead, they propose a point charge model where each DJ particle is considered as a composition of many point charges, mutual interactions of which amount to the total force between two different DJ particles. Hagy and Hernandez[31,32] have constructed a point-wise (PW) model that is smooth and therefore allows for the simulation of static and dynamical properties of Janus system.

Patchy-particle models[33,36,37,40,48–52] are closely related to DJ models. In models of both systems, the repulsive/attractive nature of the particles is often treated through the application of a "switching function" to capture angular dependencies in the anisotropic potential. The latter is either found by fitting simulation data[51,52] or performing analytical treatment.[50] It has also been benchmarked against experimental data.[52] Unfortunately, the discontinuous nature of the "switching function" makes them difficult to characterize dynamical behavior.

On the other hand, in the limit of uniform spheres, the Derjaguin approximation (DA)[53–56] offers an approximate smooth expression. The resulting analytical function relates the potential between two spheres to that of two parallel infinite plates through an approximate mapping. Thus, once the potential between two parallel plates is found, an expression for two spheres can be calculated. For example, Ohshima[57] used the DA to develop a soft step function model for the potential between two plates using Debye-Huckel and Poisson-Boltzmann equations. It was also applied[50] to DJ particles in a specific case to resolve the Casimir interaction at the critical temperature T_c.

Despite significant attention on DJ particles, its nonuniform surfaces poses a serious challenge to the construction of the smooth potentials needed in particle dynamics models to obtain spatial and temporal resolution. In this work, we demonstrate the use of a modified

DA method to construct the interaction between two DJ particles from the bottom up. It allows one to uncover the effects from anisotropy, and avoids the explicit use of a multipole expansion. It also reduces the computational time significantly. We compare our theoretical model with the brute-force computational approach involving the many pairwise interactions between DJ particles modeled at the PW scale following the same procedure adopted by Hagy and Hernandez.[31,32]

2 Methods: Theory

2.1 Interaction potential

The total interaction potential between two arbitrary DJ spherical particles, denoted 1 and 2, in a solution can be written as

$$U_{\mathrm{DJ}}(r, \mathbf{n}_1, \mathbf{n}_2) = u_{\mathrm{rep}}(r) + u_{\mathrm{elec}}(r, \mathbf{n}_1, \mathbf{n}_2)\,, \tag{1}$$

where $u_{\mathrm{rep}}(r)$ is an isotropic repulsive interaction depending only on the distance r between the centers of the particles and $u_{\mathrm{elec}}(r, \mathbf{n}_1, \mathbf{n}_2)$ is the electrostatic potential between them. The latter depends both on the distance between the spheres and their relative orientations, which are described by the unit vectors $\mathbf{n}_1$ and $\mathbf{n}_2$ corresponding to their normalized dipole momenta (see Sec. 2.3 for more details). In the present case, $u_{\mathrm{rep}}(r)$ takes the form of a shifted WCA[58]-like potential including only the repulsive part of the Lennard-Jones potential shifted by the distance Δ and truncated at the energy minimum $r_{\min} = \Delta + 2^{1/6}\sigma$. Specifically, it takes the purely repulsive form,

$$u_{\mathrm{rep}}(r) = \left(4\,u_0 \left[\left(\frac{\sigma}{r-\Delta} \right)^{12} - \left(\frac{\sigma}{r-\Delta} \right)^{6} \right] + u_0 \right) \Theta(r_{\min} - r)\,, \tag{2}$$

where $\Theta(x)$ is the usual Heaviside step function which goes from 0 to 1 at the origin. The form of Eq. (2) is chosen due to its tunability to the amplitude, slope and the cut-off distance of the repulsive potential with a minimum of adjustable parameters. The effective repulsive diameter D obeys the condition

$$u_{\rm rep}(D) = k_{\rm B}T\,. \tag{3}$$

The temperature T is set at 300 K throughout. For numerical calculations, the geometric parameters are chosen from our earlier work[31,32] modeling DJ with a discretization of their surfaces using a PW model. Specifically, $D = 220$ nm, $\sigma = 50$ nm and $\Delta = 170$ nm. Hence, the form of Eq. (2) suggests that $u_{\rm rep}(r) = 0$ if $r \geq r_{\rm min} \approx 226.1$ nm, and the condition in Eq. (3) implies that $u_0 = k_{\rm B}T/\left(1 - 2[\sigma/(D-\Delta)]^6\right)^2 = k_{\rm B}T$. The width of the nontrivial part of the repulsive potential, $r_{\rm min} - D$, constitutes around 3% of the diameter in our case. This is relatively small and consistent with that seen in experiments.[59,60]

The current work is focused on developing an analytical expression for the electrostatic potential part, $u_{\rm elec}(r, \mathbf{n}_1, \mathbf{n}_2)$, within the framework of the DA. We will denote it U for both simplicity and distinguishing it from the rigorous PW model, Eq. (30). The repulsive interaction is used in the free energy calculations only (Sec. 3.2.2).

2.2 Derjaguin's approximation

The DA in the DLVO theory allows one to derive the potential energy between two spheres from the potential energy between two parallel plates. According to it, each sphere is assumed to be made of an infinite number of rings with infinitesimal dimension. The sum-total of potentials between all these rings constitutes the final result for the potential between the spheres.

For the potential energy of two isotropic spheres with radii a_1 and a_2, the DA gives[53–56,61]

$$U = \frac{2\pi a_1 a_2}{a_1 + a_2} \int_H^\infty V_{\rm pl}(h)\, dh\,, \tag{4}$$

where H is the distance of closest approach between the surfaces of the spheres, and $V_{\rm pl}(h)$ is the interaction energy (related to the unit area) between two parallel infinitesimally small opposing annular rings directly facing each other separated by a distance h. The assumption about the short interaction range enables the upper integration limit to be extended to infinity in usual practice. However, the actual limit is $H + a_1 + a_2$, and for practical reasons, we will use this limit for the integration in Eq. (4):

$$U = \frac{2\pi a_1 a_2}{a_1 + a_2} \int_H^{H+a_1+a_2} V_{\rm pl}(h)\, dh\,. \tag{5}$$

Since beyond this upper limit the contribution of the potential is insignificant, its use does not change the result. In the case of identical particles, $a_1 = a_2 = a$, the potential reduces to

$$U = \pi a \int_H^{H+2a} V_{\rm pl}(h)\, dh\,. \tag{6}$$

For simplicity, below we continue to define the energy $V_{\rm pl}$ for the interaction between two parallel unit plates which have the same charge densities including signs in all of the cases considered below. Because of this definition, $V_{\rm pl}$ is always positive. In the next section, the DJ anisotropy will be incorporated in the integral in Eq. (6) through a multiplier which cuts off a part of the contribution from the energy $V_{\rm pl}$ due to fact that negative and positive charges seen in the general case partially offset.

2.3 Modified Derjaguin's approximation for Janus interactions

We now develop the theoretical expression for the potential energy between two DJ particles. The strategy is inspired by the DA approximation in which we consider the directly facing annuli from each DJ particle and map them to the corresponding planes. In the simplest case, each annuli are uniform with the same charge, but as particles are rotated, they will have multiple regions with alternating sign. In what follows, we consider the different relative rotations of the DJ particles going from cases with the simplest such overlaps to the most

complicated case for an arbitrary rotation.

To begin, let's consider Janus particles in three dimensions, as they are shown in Fig. 1. For each particle, the dividing plane (DP) divides the sphere into two hemispheres: positively (red) and negatively (blue) charged, each having an even surface charge density with an absolute value ρ. The total positive and negative charges are

$$\begin{aligned} q_+ &= 2\pi a^2 \rho \equiv q/2 \\ q_- &= -2\pi a^2 \rho \equiv -q/2 \end{aligned} \tag{7}$$

The unit vector $\mathbf{n}$ is perpendicular to the DP and is parallel to the dipole moment of the particle.

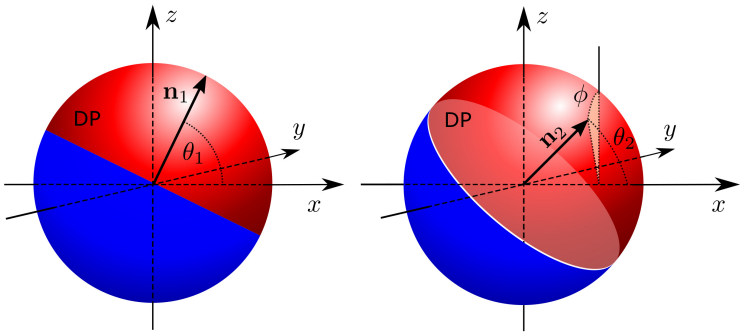

Figure 1: Orientation coordinates of two Janus particles relative to the structure in which the DP —which divides oppositely charged hemispheres— is orthogonal to the x axis. At left, the DP is only rotated around the y axis, and at right, the DP is first rotated around the y axis and then the x axis. The vectors $\mathbf{n}_i$ for $i \in (1, 2)$ are normal to their respective DP and make an angle θ_i with the x-axis; ϕ is the azimuthal angle describing the rotation of $\mathbf{n}_2$ around the x-axis. Each θ_i spans the area between $-\pi$ and π; ϕ goes around the ring from 0 to 2π.

The relative configuration of the DJ colloids placed along the x-axis can be described by a set of four coordinates $(H, \theta_1, \theta_2, \phi)$ in indicated in Fig. 1. Here, $\theta_i \in [-\pi, \pi]$ is the angle between the vector $\mathbf{n}_i$ and the x-axis, and $\phi \in [0, 2\pi]$ is the azimuthal angle between the z-axis and the plane spanned by the vector $\mathbf{n}_2$ and x-axis. The vector $\mathbf{n}_1$ always lies in the xz-plane, so that the azimuthal angle for the first particle is always 0. In the parametric space $(\theta_1, \theta_2, \phi)$ describing the relative orientation, the transformation $\mathbf{n}_i \to -\mathbf{n}_i$ is equivalent

to $\theta_i \to \theta_i - \pi$ with ϕ kept constant.

The potential U calculated within the DA necessarily satisfies the conditions obeyed by the electrostatic potential:

$$\begin{aligned} u_{\rm elec}(r, \mathbf{n}_1, \mathbf{n}_2) &= u_{\rm elec}(r, \mathbf{n}_2, \mathbf{n}_1) \\ u_{\rm elec}(r, \mathbf{n}_1, \mathbf{n}_2) &= -u_{\rm elec}(r, -\mathbf{n}_1, \mathbf{n}_2) \\ u_{\rm elec}(r, \mathbf{n}_1, \mathbf{n}_2) &= -u_{\rm elec}(r, \mathbf{n}_1, -\mathbf{n}_2)\,. \end{aligned} \tag{8}$$

2.3.1 Case 1: Axial symmetry

When $\theta_1 = \pi$ and $\theta_2 = 0$, as shown in Fig. 2A, the potential takes the form of Eq. (6) with positive values of $V_{\rm pl}(h)$. If both angles are equal to π (or 0) (Fig. 2B), then the potential changes its sign. The general expression for the potential in this case can be written as

$$U = -\pi a \cdot \mathrm{sign}(\cos\theta_1 \cos\theta_2) \int_H^{H+2a} V_{\rm pl}(h)\, dh\,, \tag{9}$$

where the function, sign$(\cdot)$, in the prefactor defines whether the potential is positive or negative, depending on the mutual orientation of the vectors $\mathbf{n}_1$ and $\mathbf{n}_2$.

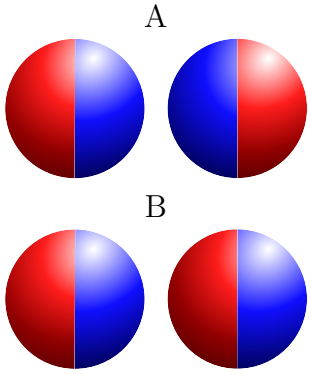

Figure 2: Relative orientations of pairs of Janus particles in the case of axial symmetry (case 1) when the facing surfaces either have the same charge (panel A) or have opposite charge (panel B).

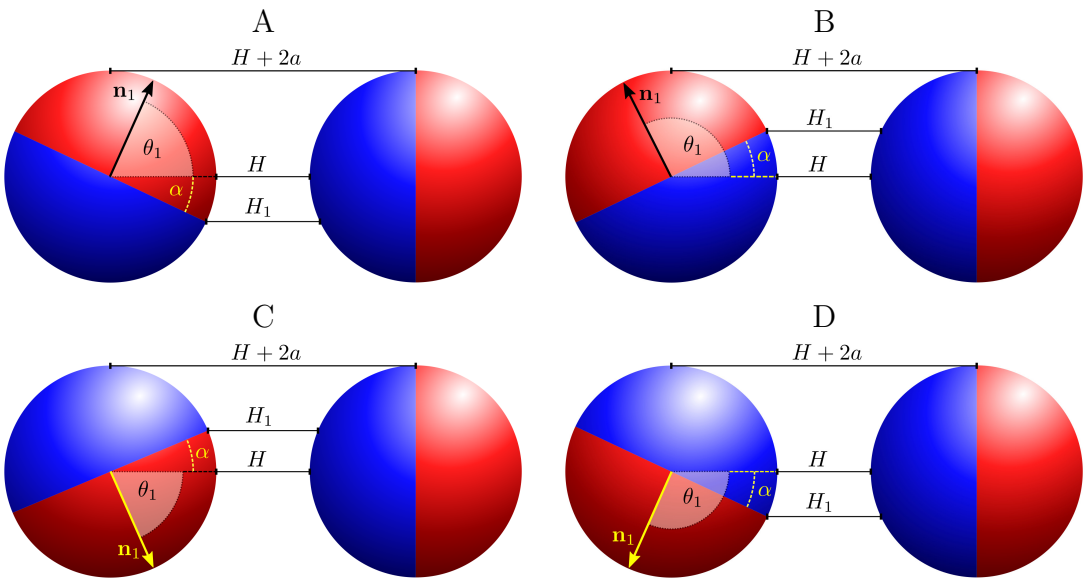

Figure 3: Relative orientations of Janus particles in case 2 when the left particle rotates around the y axis, and the right particle remains fixed with its DP orthogonal to the x axis. Panel A: $0 < \theta_1 < \pi/2$. Panel B: $\pi/2 < \theta_1 < \pi$. Panel C: $-\pi/2 < \theta_1 < 0$. Panel D: $-\pi < \theta_1 < -\pi/2$. The values of α are kept the same. H is the minimal distance between the surfaces; H_1 is the distance between the point on the DP of the left particle, which is the closest to the right particle, and an opposing point on the right particle; a is the particles' radius.

2.3.2 Case 2: Fixed $\theta_2 = 0$ (or $\theta_2 = \pi$)

We now consider the case when one of the particles is fixed with its DP perpendicular the x axis (that is, when θ_2 equal 0 or π), and the other particle is allowed to rotate with varying θ_1 for $\phi = 0$. Figures 3A-D show four different orientations of the vector $\mathbf{n}_1$ within four quadrants of the xz-plane in which the (positive) angle $\alpha = ||\theta_1| - \pi/2|$ has the same value, and $\theta_2 = 0$. The distance H_1 is the same in all four of these orientations and given by

$$H_1 = H + 2a(1 - \cos\alpha) = H + 2a(1 - |\sin\theta_1|)\,. \tag{10}$$

Due to symmetry, the interaction energies corresponding to these configurations have the same absolute values but may have different signs. We first derive the expression for the energy in reference to the configuration shown on panel A of Fig. 3, and then generalize for three other possible orientations by including for the appropriate sign.

The strategy for determining the total energy through successive integration over the corresponding rings (or annuli) is illustrated in Fig. 4 for the case in which there are three different overlapping cross sections of particle 1. We introduce angle $\gamma \in [0, \pi/2]$ as it uniquely identifies each cross section and simplifies the formulas. In Fig. 4, this angle also marks location of the BB_1 ring. The distance h between the opposite rings on the spheres is connected to angle γ as

$$h = H + 2a(1 - \sin\gamma) \, . \tag{11}$$

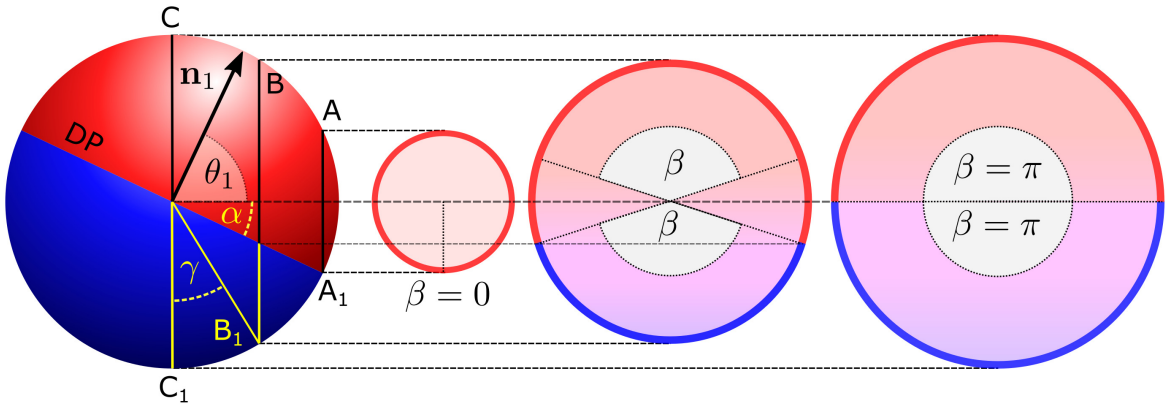

Figure 4: Particle 1 (left) and its cross sections AA_1, BB_1 and CC_1 (three annular rings on the right). The sections which correspond to the negatively charged part of each ring are denoted by angle β. The AA_1 ring defined by the lower point of the DP is fully positively charged (thus $\beta = 0$); together with its negative counterpart ring on particle 2 (not shown), it contributes to the attraction part of the energy U. The BB_1 ring has both negative and positive charges. The CC_1 ring is the largest cross section. It is half positively and half negatively charged.

The integration procedure is subdivided into two steps. The first step integrates the energy $V_{\rm pl}(h)$ from distance H to H_1 (γ changes from $\pi/2$ to $\pi/2 - \alpha$). At this stage fully positively charged red rings of particle 1 face matching fully negatively charged blue rings of particle 2. The interaction between these rings contribute to the integral giving the first —negative— term of Eq. (13). Second, when h changes from H_1 to $H + 2a$ (and γ changes from $\pi/2 - \alpha$ to 0), rings of particle 1 bear charges of both signs, whereas adjacent rings of particle 2 are all negatively charged. Thus, only a part of the interaction of those rings

contributes to the result. This part is

$$\chi_1 = (2\pi - 2\beta)/2\pi\,, \tag{12}$$

since the upper and lower segments cancel each other (see the BB_1 and CC_1 annuli in Fig. 4). These annuli give the second —also negative— term of Eq. (13):

$$U = -\pi a \int_H^{H_1} V_{\rm pl}(h)\, dh - \pi a \int_{H_1}^{H+2a} V_{\rm pl}(h)\, \chi_1(\gamma) dh\,, \tag{13}$$

where the value of χ_1 can be expressed via γ as (see Sec. S1 in the Supporting Information (SI))

$$\chi_1(\gamma) = \frac{2}{\pi} \sin^{-1}(\tan\gamma \cdot |\cot\theta_1|) \tag{14}$$

and γ is a function of h, according to Eq. (11).

For an arbitrary value of the angle θ_1 and two possible orientations of colloid 2—which in this subsection correspond to $\theta_2 = 0$ and $\theta_2 = \pi$—Eq. (13) can be recast as

$$U = -\pi a \cdot \text{sign}\,(\cos\theta_1 \cos\theta_2) \left(\int_H^{H_1} V_{\rm pl}(h)\, dh + \int_{H_1}^{H+2a} V_{\rm pl}(h)\, \chi_1(\gamma) dh \right)\,, \tag{15}$$

where the sign$(\cdot)$ is defined as in Eq. 9, and in accordance with conditions (8).

2.3.3 Case 3: Arbitrary θ_1 and θ_2 at $\phi = 0$

We now relax the constraint on the fixed particles imposed in case 2, and allow both particles to rotate around their symmetry axes—that is y. As indicated in Fig. 5, three regions of integration are now needed for the calculation of the energy U. Let's assume that both vectors $\mathbf{n}_1$ and $\mathbf{n}_2$ are in the first quadrant, and $\theta_1 > \theta_2$, which makes $H_1 < H_2$. The first two regions are similar to those from the previous section, except the upper integration limit in the second term is now $H_2 = H + 2a(1 - |\sin\theta_2|)$. In the third (and last) region, the integration is performed from H_2 to $H + 2a$, where all adjacent rings of both spheres bear

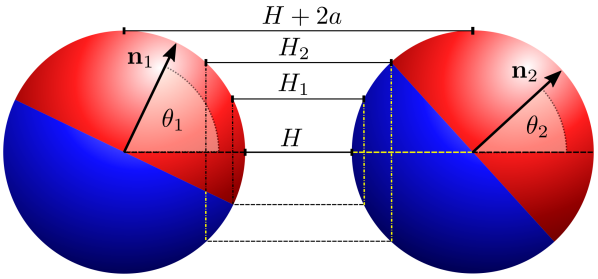

Figure 5: Relative orientations of Janus particles in case 3 when both particles rotate around the y axis with arbitrary values of θ_1 and θ_2. The distances H, H_1 and a are the same as in Fig. 3; H_2 is the distance between the point on the DP of the right particle, closest to the left particle, and an opposing point on the left particle.

charges with different signs. Thus,

$$U = -\pi a \left(\int_H^{H_1} V_{\rm pl}(h)\, dh + \int_{H_1}^{H_2} V_{\rm pl}(h)\, \chi_1(\gamma) dh \right) + \pi a \int_{H_2}^{H+2a} V_{\rm pl}(h)\, \chi_2(\gamma) dh \,. \tag{16}$$

The second kernel χ_2 is derived in Sec. S2 of the SI and takes the form:

$$\chi_2(\gamma) = 1 - \frac{2}{\pi} \left(\sin^{-1}(\tan\gamma \cdot |\cot\theta_1|) + \sin^{-1}(\tan\gamma \cdot |\cot\theta_2|) \right) \tag{17}$$

Taking into account all the possible orientations of the particles within the xz-plane, the whole potential, according to conditions (8), takes the form

$$U = \pi a \left(-\mathrm{sign}(\cos\theta_1 \cos\theta_2) \int_H^{H_-} V_{\rm pl}(h)\, dh \right. \tag{18a}$$

$$- \mathrm{sign}(\cos\theta_1 \cos\theta_2) \int_{H_-}^{H_+} V_{\rm pl}(h)\, \chi_1(\gamma) dh \tag{18b}$$

$$\left. + \mathrm{sign}(\sin\theta_1 \sin\theta_2) \int_{H_+}^{H+2a} V_{\rm pl}(h)\, \chi_2(\gamma) dh \right) \,, \tag{18c}$$

where $H_- = \min(H_1, H_2)$, $H_+ = \max(H_1, H_2)$ and the first kernel is now defined by the minimal distance H_- as

$$\chi_1(\gamma) = \frac{2}{\pi} \sin^{-1} \left(\tan\gamma \cdot \min\left(|\cot\theta_1|, |\cot\theta_2| \right) \right) \,. \tag{19}$$

2.3.4 The general case

We now allow all possible rotations of both of the particles as indicated in Fig. 1. Although, the special cases considered in the preceding sections sever to confirm the limiting cases of this result, and they also helped define the terms that are useful in this gereralized case.

Using the same subdivision of the regions on integration employed in the previous section, it is easy to see that first two terms, which correspond to the overall integration from H to H_2, according to Fig. 5 and Eq. (16) (or from H to H_+, according to Eqs. (18a)-(18b)), are not affected by the rotation about the x-axis, since at least one of the adjacent rings is monotonic, *i.e.*, fully positively or fully negatively charged. Namely,

$$U = \pi a \left(-\text{sign}(\cos\theta_1 \cos\theta_2) \int_H^{H_-} V_{\text{pl}}(h)\, dh \right. \tag{20a}$$

$$- \text{sign}(\cos\theta_1 \cos\theta_2) \int_{H_-}^{H_+} V_{\text{pl}}(h)\, \chi_1(\gamma) dh \tag{20b}$$

$$\left. + \text{sign}(\sin\theta_1 \sin\theta_2) \int_{H_+}^{H+2a} V_{\text{pl}}(h)\ (\chi_2(\gamma) + \Delta\chi_2(\gamma,\phi))\, dh \right) , \tag{20c}$$

The third term is the only one which depends on ϕ. The detailed derivation of the correction $\Delta\chi_2$ to χ_2 is provided in Sec. S3 of the SI, and amounts to:

$$\Delta\chi_2(\gamma,\phi) = \frac{1}{\pi} \left(\left| \nu - \frac{|\beta_1 - \beta_2|}{2} \right| - \left| \nu - \frac{\beta_1 + \beta_2}{2} \right| - \min(\beta_1, \beta_2) \right) , \tag{21}$$

where $\nu(\phi) = ||\phi| - \pi|$ and $\beta_{1,2}(\gamma) = 2\cos^{-1}(\tan\gamma \cdot |\cot\theta_{1,2}|)$. Equation (20) with Eqs. (19), (17) and (21) constitute our main result. Substituting a correct form of the function $V_{\text{pl}}(h)$ (described in the next section) fulfills our goal to construct the Derjaguin potential energy for DJ colloids.

Generally speaking, the size of the contribution of the three terms in Eq. (20), decreases from (20a) to (20c). This is because the contribution of each term is defined by a particular stage of integration: $h \in [H, H_-]$, $h \in [H_-, H_+]$ and $h \in [H_+, H + 2a]$. The first stage corresponds to the interaction of charged spherical segments with the same charge; the

second stage occurs when the charge of parts of one of the segments starts to flip so that its variation in charge stands in opposition to the other uniformly-charged segment; and the third stage contains segments with charges that vary both particles. As we move through these stages, the value of $V_{\rm pl}(h)$ becomes smaller because the points on the segments are farther away. In addition, the factors χ_1, χ_2 and $\Delta\chi_2$ reduce the amplitude of the interaction potential. The accuracy of the approximation is less for stages which include non-uniformly charged segments because our implementation of Derjaguin's approach in the context of DJ particles assumes uniformly charged segments. However, as these are precisely the terms that are small, the overall approximation of the interaction term between the DJ particles can be quite good as we report below.

3 Results & Discussion

3.1 The effective potential between planar surfaces for nonuniform spherical surfaces

The interaction energy between DJ particles aligned as in Figure 2B is equivalent to the interaction between uniform spheres, and hence the usual DA is applicable directly. Once the DJ particles rotate, the faces are no longer uniform and the results of the previous section provide an estimate of how the interactions are effectively modified by the sum of contributions with mixed sign. However, we still need an estimate for the potential between planar surfaces, $V_{\rm pl}(h)$ of Eqs. (4)-(6), that effectively renormalizes the contributions from the original potential between spherical surfaces, and that is what is elaborated here.

The screened Coulomb potential for small ions is known from Debye–Hückel theory:

$$dU_{\rm DH}(r) = \frac{dq_i dq_j}{4\pi\epsilon_0\epsilon r}\frac{e^{-\kappa r}}{(1+\kappa a_i)(1+\kappa a_j)}\,, \tag{22}$$

where $dq_{i(j)}$ is the charge of ion $i(j)$, $a_{i(j)}$ is its radius, κ is the reciprocal screening length,

r is the distance between the ions, ϵ_0 is the absolute permittivity and ϵ_r is the permittivity of the medium. The latter is chosen to correspond to pure water, $\epsilon = 80.1$.

A discretization (or tiling) of the surface of a colloidal particle into infinitesimally small charges (such that $a_{i(j)} = 0$) located on the surface provides a basis for constructing the overall interaction between the spheres as an integration between the charges. This integration over the two surfaces (similar to those performed in Ref. 57) gives the following expression for the screened Coulomb potential for identical spherically-symmetric colloids:

$$U_{\mathrm{DH}}(r) = \frac{q^2}{4\pi\epsilon_0\epsilon r} e^{-\kappa r} \left(\frac{\sinh(\kappa a)}{\kappa a} \right)^2 , \tag{23}$$

where q is the total charge of a particle, and $r = H + 2a$ is the distance between the centers of colloids.

On the other hand, the DA in Eq. (6) can also be used to calculate the energy. One only needs the interaction energy per unit area between two plates, $V_{\mathrm{pl}}(h)$, which must first be found. For the elementary potential (22), when the charge is uniform across the spheres, $V_{\mathrm{pl}}(h)$ has an exponential form[57]

$$V_{\mathrm{pl}}(h) = Ae^{-\tilde{\kappa}h} , \tag{24}$$

where A is a constant proportional to the prefactors in Eq. (22) and $\tilde{\kappa}$ is equal to κ.[57] Our strategy is thus to introduce a renormalization in which we redefine the parameters A and $\tilde{\kappa}$ in such a way as to obtain the correct result (23) after substituting $V_{\mathrm{pl}}(h)$ into Eq. (6).

The integration of Eq. (6) with $V_{\mathrm{pl}}(h)$ from Eq. (24) gives

$$U(H) = \pi a A \tilde{\kappa}^{-1} e^{-\tilde{\kappa}H} (1 - e^{-2\tilde{\kappa}a}) . \tag{25}$$

The parameters A and $\tilde{\kappa}$, not specified in Eqs. (24) and (25), can now be obtained by equating potential energies (23) and (25) and their derivatives at the same interparticle distance:

$$U_{\mathrm{DH}}(H + 2a) = U(H) \tag{26}$$

$$dU_{\mathrm{DH}}(H+2a)/dH = dU(H)/dH \tag{27}$$

The result is

$$\tilde{\kappa} = \kappa + \frac{1}{H+2a} \tag{28}$$

$$A = \frac{q^2}{4\pi\epsilon_0\epsilon}\,\frac{\tilde{\kappa}}{\pi a(H+2a)}\,\frac{e^{1-2\tilde{\kappa}a}}{1-e^{-2\tilde{\kappa}a}}\left(\frac{\sinh(\kappa a)}{\kappa a}\right)^2, \tag{29}$$

where the charge is defined via the charge density as $q = 4\pi a^2\rho$.

Substitution of Eqs. (28) and (29) back into Eq. (25) immediately retrieves the Debye–Hückel equation (23). The purpose of the renormalization is to make Eqs. (15), (18) and (20), with the orientation-dependent factors χ_1, χ_2 and $\Delta\chi_2$ taken into account, as close to the correct electrostatics as possible. All the integrations can now be performed numerically for different orientations and distances.

3.2 Comparison between theory and bottom-up constructions

To verify our analytical result numerically, we have adopted a rigorous PW[31] model, where the electrostatic interaction in Eq. (1) is calculated as follows. We consider $n = 2000$ point charges evenly distributed across the spherical surfaces of each particle in a pair. The potential energy takes the form

$$u_{\mathrm{elec}}(r, \mathbf{n}_i, \mathbf{n}_j) = \frac{q_0^2}{4\pi\epsilon_0\epsilon_r}\sum_i^n\sum_j^n s_i s_j c(|\mathbf{p}_i - \mathbf{p}_j|)\,, \tag{30}$$

$$c(x) = e^{-\kappa x}/x\,, \tag{31}$$

where $\{\mathbf{p}_i\}$ and $\{\mathbf{p}_j\}$ represent the positions of point charges on the first and second spheres. Each point has a charge magnitude of $q_0 = q/n$ (see Eq. (7)) and a charge sign of $s = \pm 1$ to model the positive and negative hemispheres of a DJ particle.

The surface density is calculated via Eq. (7) with $a = 100$ nm. Its values listed in Table 1 correspond to the screening lengths $\kappa^{-1} = 5$, 10 and 20 nm and the free energy minima

$A_{\min}/k_{\mathrm{B}}T = -1$, -2 and -3 (see Sec. 3.2.2).

3.2.1 The modified DA Electrostatic Potential

The PW (curves) and modified-DA (symbols) electrostatic potentials as a function of distance at several fixed mutual orientations are compared. Because of symmetry, we need only focus on two orientations θ_1 of the first particle while varying the orientation of the second particle:

(i) When $\theta_1 = 0$, a single positively charged hemisphere of particle 1 points toward particle 2. A comparison of the resulting PW and modified-DA electrostatic potentials for various orientations of the second particle (θ_2) are shown in Figs. 6A, 6C and 6E for three representative screening lengths, respectively. When $\theta_2 = 0^\circ$ or 45°, for example, the two DJs particles face each other primarily through uniformly charged surfaces. Consequently, the interaction is then determined by the most significant and accurate term (20a) of the potential energy. The modified-DA and PW results are almost indistinguishable. When $\theta_2 = 75^\circ$, the less-accurate second term in Eq. (20) starts to contribute to the result, and leads to a deviation between the PW and modified-DA. At $\theta_2 = 90^\circ$, the interaction reduces to zero because of the T-shaped geometry. In between $\theta_2 = 75^\circ$ and $\theta_2 = 90^\circ$, use of Eqs. (20a) and (20b) provides an effective potential that interpolates well between these limits as can be seen in Fig. S5A in the SI.

(ii) When the angle $\theta_1 = 90^\circ$, the first two terms in Eq. (20) vanish, and the modified-DA is at its worse. The resulting PW and modified-DA electrostatic potentials for various orientations of the second particle (θ_2) are shown in Figs. 6B, 6D and 6F for three representative screening lengths, respectively. When $\theta_2 = 0^\circ$ or 45°, for example, the T-shaped geometry leads to vanishing values of the energy and now corresponds exactly to $\theta_2 = 0^\circ$ (black) and practically to 45° (blue). The deviations across the entire range of θ_2 are shown in Fig. 7D. At $\theta_2 = 90^\circ$ (270°) when both dipoles are perpendicular to the x-axis and parallel to each other, so that the edges of the DPs of the Janus particles are directly opposed, the difference between the modified-DA and PW becomes most noticeable. Namely, the modified-DA leads

to higher (lower in the case of 270°) energies. Therein, the modified-DA approach accounts only for the oppositely located surface areas, omitting the crossed-area interactions. Since the opposed areas have charges of the same sign (or opposite sign in the case of a 270° orientation), the calculated energy is equivalent to the orientation with $\theta_1 = 0°$ and $\theta_2 = 180°$ (or $\theta_1 = \theta_2 = 0°$). Thus, certain relative orientations will be avoided by the Janus particles during MD simulations while other orientations will be preferred.

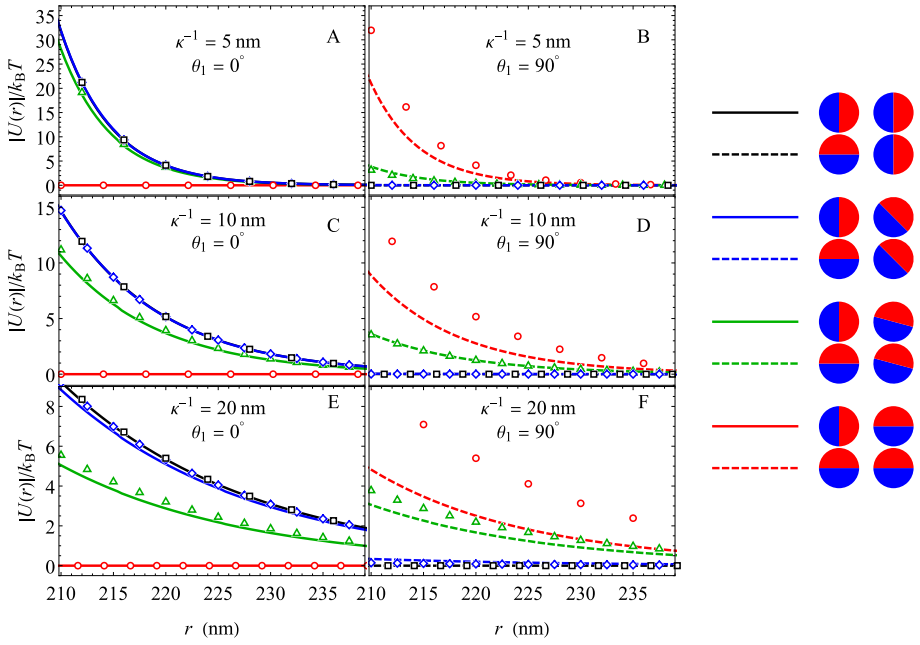

Figure 6: Comparison of the electrostatic potential between the modified-DA of Eq. 20 (curves) and the PW calculation of Eq. (30) (symbols) in units of k_BT as a function of r at $H = 10$ nm, $\phi = 0°$ and different values of θ_1, θ_2 and κ. The relative orientation of the spheres in each case is shown in the legend at the right, with the left and right spheres indicating the angles θ_1 and θ_2, respectively. The values of κ and θ_1 are indicated in each panel. Colors indicate the angle, θ_2 of the sphere at the right: black for $\theta_2 = 0°$, blue for $\theta_2 = 45°$, green for $\theta_2 = 75°$, and red for $\theta_2 = 90°$. The charge density corresponds to $A_{\min} = -3\,k_BT$. (see Fig. 8 and Table 1).

In between these two limiting cases, the modified-DA is a good approximation to the PW electrostatic potential as shown in Fig. 7. Notably, the modified-DA is better with decreasing Debye length, but appears to be good enough to characterize a broad range of interaction distances and orientations. The cases when the edges of the DPs of the Janus particles are directly opposed lead to peaks in the electrostatic potential (see Figs. 7C-E). The absence of smoothing from the modified-DA in these cases is reflected in small deviations that are

suppressed in the overall potential of mean forces (PMFs) reported below.

3.2.2 Potential of mean force

The PMF is calculated according to

$$A(r) = -k_{\mathrm{B}}T \ln \left\langle e^{-U_{\mathrm{DJ}}(r,\mathbf{n}_1,\mathbf{n}_2)/k_{\mathrm{B}}T} \right\rangle , \tag{32}$$

where U_{DJ} includes both isotropic repulsive and screened electrostatic potential energy and the brackets denote an average over the orientations of the vectors $\mathbf{n}_1$ and $\mathbf{n}_2$. The computational times required for several cases of the modified-DA and PW calculations are shown in Table S1 in the SI, and indicate a savings from hours to minutes. As in Ref. 31, we chose 4096 different mutual orientations of these vectors. The free energy profiles at three representative screening lengths κ^{-1} are shown in Figs. 8A-C where different colors correspond to different values of the potential minimum, A_{min} as noted in the caption. The charge densities are chosen such that the free energy minima A_{min} reach $-k_{\mathrm{B}}T$, $-2\,k_{\mathrm{B}}T$ and $-3\,k_{\mathrm{B}}T$ (see Table 1 for details). As can be seen, the modified-DA (symbols) is in an excellent agreement with the PW model (curves), slightly deteriorating at the largest value of the Debye length, 20 nm. Note that the latter represents 10% of the particle's diameter—a large distance in terms of applicability of the Derjaguin approach. Similar agreement can be seen in Fig. S6 in the SI across a domain in the azimuthal angle ϕ for various values in κ and θ_2.

Table 1: The charge density, ρ, used in Fig. 8 chosen to equate the energy minima to predefined numbers at various values of κ.

Panel	κ^{-1}, nm	ρ, $10^4\,e_0/\mu\mathrm{m}^2$		
		$A_{\mathrm{min}} = -3\,k_{\mathrm{B}}T$ (Blue)	$A_{\mathrm{min}} = -2\,k_{\mathrm{B}}T$ (Red)	$A_{\mathrm{min}} = -k_{\mathrm{B}}T$ (Green)
A	5	8.5006	7.9261	7.0975
B	10	1.7498	1.5578	1.2988
C	20	0.54218	0.47467	0.38548

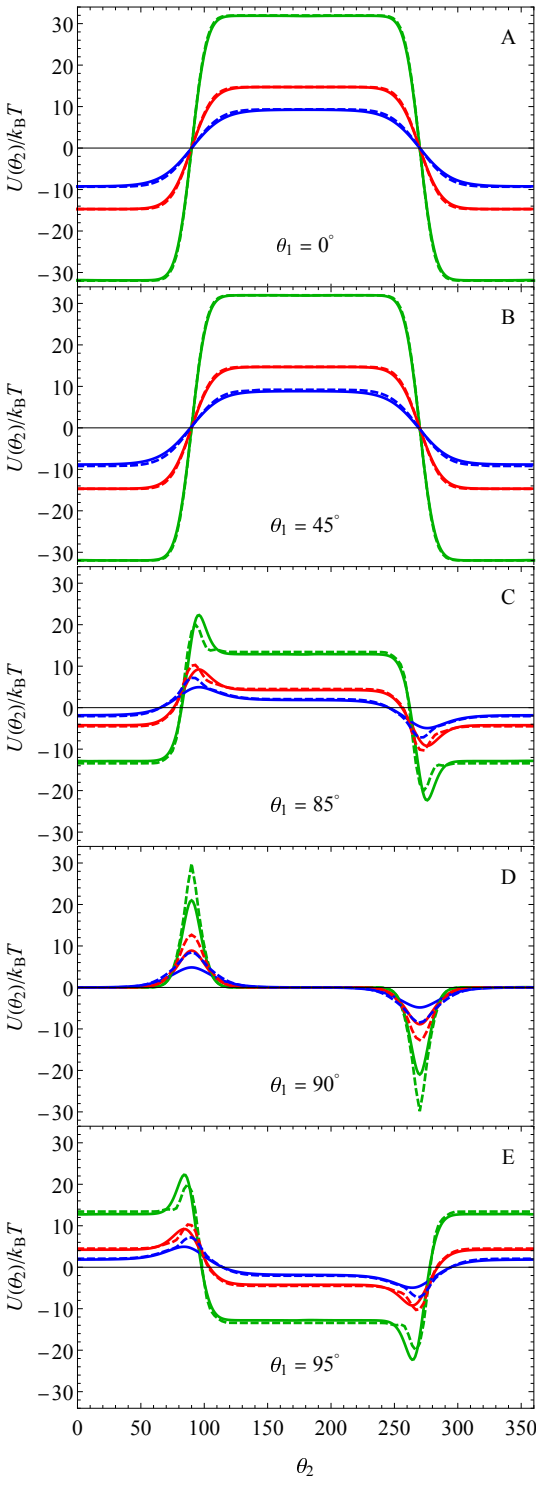

Figure 7: Electrostatic potential in the units of k_BT as a function of θ_2 at $H = 10$ nm, $\phi = 0$ and different values of θ_1 and κ. Solid lines: the PW u_{elec} from Eq. (30). Dashed lines: the modified-DA (20). Green curves: $\kappa^{-1} = 5$ nm. Red curves: $\kappa^{-1} = 10$ nm. Blue curves: $\kappa^{-1} = 20$ nm. The corresponding values of θ_1 are indicated in each panel. The charge density corresponds to $A_{min} = -3\,k_BT$ (see Fig. 8 and Table 1).

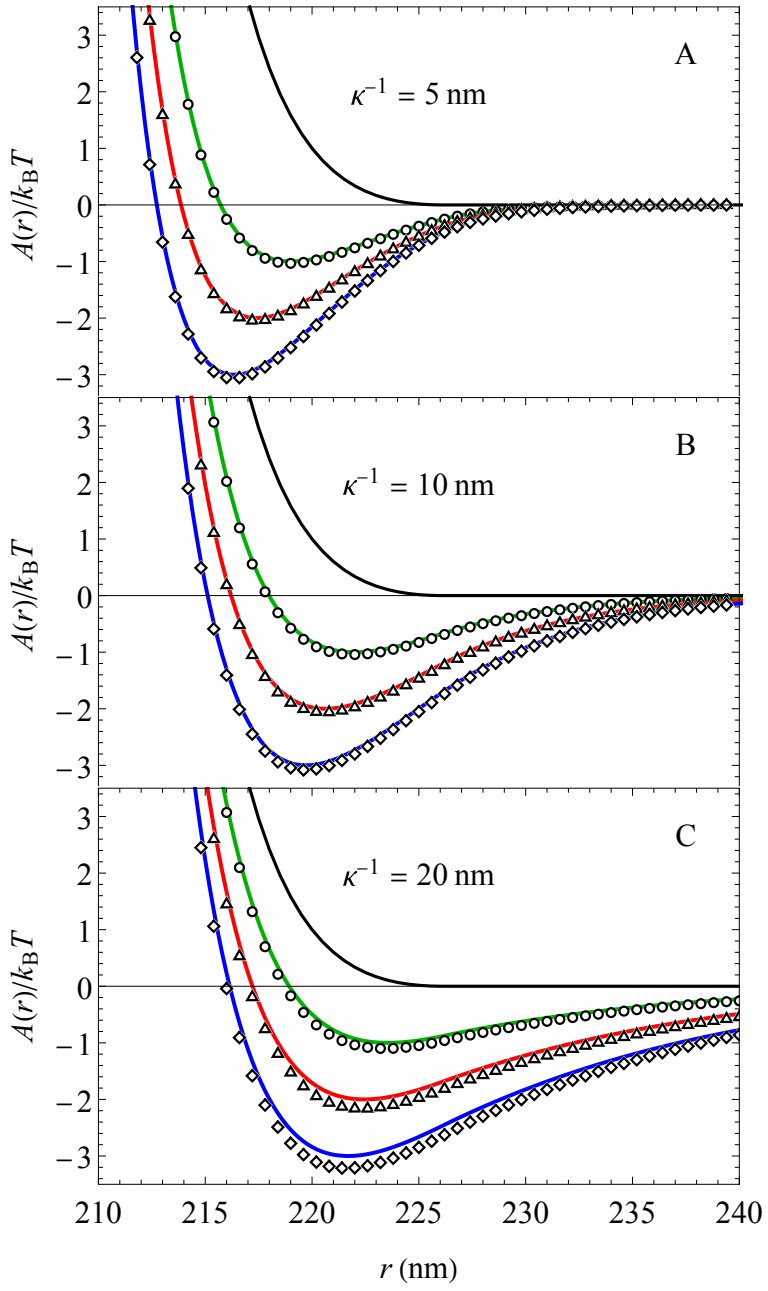

Figure 8: PMF in the units of k_BT as a function of r at different values of ρ and κ. Open symbols correspond to the modified-DA, Eq. (20), used in the overall potential energy U_{DJ}, Eq. (1). Colored curves correspond to the PW, Eq. (30), used in the overall potential energy U_{DJ}, Eq. (1). Blue curves: $A_{min} = -3\,k_BT$. Red curves: $A_{min} = -2\,k_BT$. Green curves: $A_{min} = -k_BT$. The corresponding values of κ^{-1} are indicated in each panel. Black solid curves represent the repulsive interaction, Eq. (2). (All these parameters are listed in Table 1.)

4 Concluding remarks

Motivated by the DA, we have developed a modified theory for the screened electrostatic interaction between Janus particles that extends the known form for particles with uniformly charged surfaces from the bottom up. The theory is further improved by renormalizing the interaction energy between two parallel plates according to the resulting interaction between uniformly charged spheres.

The modified-DA electrostatic potential shows very good agreement with the PW model used in earlier simulations across a wide range of screening lengths up to about 10% of the particle size and perhaps even larger. Although the resulting formulas are expressed up to a numerical quadrature, they nevertheless reduce the computation time significantly. For example, the PW calculations of the PMF which usually take hours on current processors can now be performed within a couple of minutes using the analytical form.

An equally significant result of this work is the demonstration that the phenomenological form for the interaction potential between Janus particles used in our earlier work can be obtained from the bottom-up starting at the underlying scale of pair-wise interactions between the charges on the surfaces of the DJ particles. This provides a fundamental grounding to not just our earlier PW model[31,32] but also the related discontinuous potential models.[17]

Supporting Information

Derivations of Equations (14), (17) and (21) are available as Secs. S1, S2 and S3 in the SI, respectively. Figure 7 is redisplayed as Fig. S5 in the SI grouped such that the results for the same screening length, κ^{-1}, are in the same panel. Figure S6 in the SI shows the electrostatic potential as a function of the azimuthal angle ϕ at several values of θ_1, θ_2 and κ indicating. The relative CPU times needed for the calculation of the PMF using typical current computers are included in Table S1.

Acknowledgments

This work has been partially supported by the National Science Foundation (NSF) through Grant No. CHE 2102455. The computing resources necessary for this research were provided in part by the National Science Foundation through XSEDE resources under grant number CTS090079, and the Advanced Research Computing at Hopkins (ARCH) high-performance computing (HPC) facilities supported by the NSF MRI Grant (OAC-1920103). We acknowledge the contributions of Mr. Saurov Hazarika in the early stages of this work.

References

(1) Perro, A.; Reculusa, S.; Ravaine, S.; Bourgeat-Lami, E.; Duguet, E. Design and Synthesis of Janus Micro-and Nanoparticles. *J. Mater. Chem.* **2005**, *15*, 3745–3760, DOI: 10.1039/B505099E.

(2) Glotzer, S. C.; Solomon, M. J. Anisotropy of Building Blocks and Their Assembly into Complex Structures. *Nat. Mater.* **2007**, *6*, 557–562, DOI: 10.1038/nmat1949.

(3) Grzelczak, M.; Vermant, J.; Furst, E. M.; Liz-Marzán, L. M. Directed Self-Assembly of Nanoparticles. *ACS Nano* **2010**, *4*, 3591–3605, DOI: 10.1021/nn100869j.

(4) Pawar, A. B.; Kretzschmar, I. Fabrication, Assembly, and Application of Patchy Particles. *Macromol. Rapid Commun.* **2010**, *31*, 150–168.

(5) Du, J.; O'Reilly, R. K. Anisotropic Particles with Patchy, Multicompartment and Janus Architectures: Preparation and Application. *Chem. Soc. Rev.* **2011**, *40*, 2402–2416, DOI: 10.1039/C0CS00216J.

(6) Chen, Q.; Yan, J.; Zhang, J.; Bae, S. C.; Granick, S. Janus and Multiblock Colloidal Particles. *Langmuir* **2012**, *28*, 13555–13561, DOI: 10.1021/la302226w.

(7) Shah, A. A.; Schultz, B.; Kohlstedt, K. L.; Glotzer, S. C.; Solomon, M. J. Synthesis, Assembly, and Image Analysis of Spheroidal Patchy Particles. *Langmuir* **2013**, *29*, 4688–4696, DOI: 10.1021/la400317t.

(8) Oh, J. S.; Lee, S.; Glotzer, S. C.; Yi, G.-R.; Pine, D. J. Colloidal fibers and rings by cooperative assembly. *Nat. Commun.* **2019**, *10*, 3936, DOI: 10.1038/s41467-019-11915-1.

(9) Safaie, N.; Robert C. Ferrier, J. Janus nanoparticle synthesis: Overview, recent developments, and applications. *J. Appl. Phys.* **2020**, *127*, 170902, DOI: 10.1063/5.0003329.

(10) Hong, L.; Cacciuto, A.; Luijten, E.; Granick, S. Clusters of Amphiphilic Colloidal Spheres. *Langmuir* **2008**, *24*, 621–625, DOI: 10.1021/la7030818.

(11) Sciortino, F.; Giacometti, A.; Pastore, G. Phase Diagram of Janus Particles. *Phys. Rev. Lett.* **2009**, *103*, 237801, DOI: 10.1103/PhysRevLett.103.237801.

(12) Sciortino, F.; Giacometti, A.; Pastore, G. A Numerical Study of One-Patch Colloidal Particles: From Square-Well to Janus. *Phys. Chem. Chem. Phys.* **2010**, *12*, 11869–11877, DOI: 10.1039/C0CP00504E.

(13) Fantoni, R.; Giacometti, A.; Sciortino, F.; Pastore, G. Cluster Theory of Janus Particles. *Soft Matter* **2011**, *7*, 2419–2427, DOI: 10.1039/C0SM00995D.

(14) Li, Z.-W.; Lu, Z.-Y.; Sun, Z.-Y.; An, L.-J. Model, self-assembly structures, and phase diagram of soft Janus particles. *Soft Matter* **2012**, *8*, 6693–6697, DOI: 10.1039/c2sm25397f.

(15) Fantoni, R.; Giacometti, A.; Maestre, M. A. G.; Santos, A. Phase diagrams of Janus fluids with up-down constrained orientations. *J. Chem. Phys.* **2013**, *139*, 174902, DOI: 10.1063/1.4827861.

(16) Maestre, M. A. G.; Fantoni, R.; Giacometti, A.; Santos, A. Janus fluid with fixed

patch orientations: theory and simulations. *J. Chem. Phys.* **2013**, *138*, 094904, DOI: 10.1063/1.4793626.

(17) Hong, L.; Cacciuto, A.; Luijten, E.; Granick, S. Clusters of Charged Janus Spheres. *Nano Lett.* **2006**, *6*, 2510–2514, DOI: 10.1021/nl061857i.

(18) Jiang, S.; Chen, Q.; Tripathy, M.; Luijten, E.; Schweizer, K. S.; Granick, S. Janus Particle Synthesis and Assembly. *Adv. Mater.* **2010**, *22*, 1060–1071, DOI: 10.1002/adma.200904094.

(19) Boon, N.; Gallardo, E. C.; Zheng, S.; Eggen, E.; Dijkstra, M.; van Roij, R. Screening of heterogeneous surfaces: charge renormalization of Janus particles. *J. Phys.: Condens. Matter* **2010**, *22*, 104104, DOI: 10.1088/0953-8984/22/10/104104.

(20) Tang, J. L.; Schoenwald, K.; Potter, D.; White, D.; Sulchek, T. Bifunctional Janus Microparticles with Spatially Segregated Proteins. *Langmuir* **2012**, *28*, 10033–10039, DOI: 10.1021/la3010079.

(21) de Graaf, J.; Boon, N.; Dijkstra, M.; van Roij, R. Electrostatic Interactions Between Janus Particles. *J. Chem. Phys.* **2012**, *137*, 104910, DOI: 10.1063/1.4751482.

(22) Iwashita, Y.; Kimura, Y. Orientational order of one-patch colloidal particles in two dimensions. *Soft Matter* **2014**, *10*, 7170–7181, DOI: 10.1039/C4SM00932K.

(23) Iwashita, Y.; Kimura, Y. Spatial confinement governs orientational order in patchy particles. *Sci. Rep.* **2016**, *6*, 27599, DOI: 10.1038/srep27599.

(24) Hieronimus, R.; Raschke, S.; Heuer, A. How to model the interaction of charged Janus particles. *J. Chem. Phys.* **2016**, *145*, 064303, DOI: 10.1063/1.4960424.

(25) Goyal, A.; Hall, C. K.; Velev, O. D. Phase Diagram for Stimulus-Responsive Materials Containing Dipolar Colloidal Particles. *Phys. Rev. E* **2008**, *77*, 031401, DOI: 10.1103/PhysRevE.77.031401.

(26) Miller, M. A.; Blaak, R.; Lumb, C. N.; Hansen, J. P. Dynamical Arrest in Low Density Dipolar Colloidal Gels. *J. Chem. Phys.* **2009**, *130*, 114507, DOI: 10.1063/1.3089620.

(27) Liarte, D. B.; Salinas, S. R. Bethe-lattice calculations for the phase diagram of a two-state Janus gas. *J. Stat. Mech.* **2015**, *2015*, P02020, DOI: 10.1088/1742-5468/2015/02/p02020.

(28) Maestre, M. A. G.; Santos, A. One-dimensional Janus fluids. Exact solution and mapping from the quenched to the annealed system. *J. Stat. Mech.* **2020**, *2020*, 063217, DOI: 10.1088/1742-5468/ab900d.

(29) Kalapurakal, R. A. M.; Mani, E. Orientation-dependent electrostatic interaction between inverse patchy colloids. *Mol. Sim.* **2022**, *48*, 176–184, DOI: 10.1080/08927022.2021.1998487.

(30) Erdmann, T.; Kröger, M.; Hess, S. Phase Behavior and Structure of Janus Fluids. *Phys. Rev. E* **2003**, *67*, 041209.

(31) Hagy, M. C.; Hernandez, R. Dynamical Simulation of Dipolar Janus Colloids: Equilibrium Structure and Thermodynamics. *J. Chem. Phys.* **2012**, *137*, 044505, DOI: 10.1063/1.4737432.

(32) Hagy, M. C.; Hernandez, R. Dynamical Simulation of Dipolar Janus Colloids: Dynamical Properties. *J. Chem. Phys.* **2013**, *138*, 184903, DOI: 10.1063/1.4803864.

(33) Blanco, M. A.; Shen, V. K. Effect of the surface charge distribution on the fluid phase behavior of charged colloids and proteins. *J. Chem. Phys.* **2016**, *145*, 155102, DOI: 10.1063/1.4964613.

(34) Dempster, J. M.; de la Cruz, M. O. Aggregation of Heterogeneously Charged Colloids. *ACS Nano* **2016**, *10*, 5909–5915, DOI: 10.1021/acsnano.6b01218.

(35) Kharazmi, A.; Priezjev, N. V. Molecular Dynamics Simulations of the Rotational and Translational Diffusion of a Janus Rod-Shaped Nanoparticle. *J. Phys. Chem. B* **2017**, *121*, 7133–7139, DOI: 10.1021/acs.jpcb.7b03720.

(36) Reinhart, W. F.; Panagiotopoulos, A. Z. Crystal growth kinetics of triblock Janus colloids. *J. Chem. Phys.* **2018**, *148*, 124506, DOI: 10.1063/1.5021347.

(37) Eslami, H.; Bahri, K.; Müller-Plathe, F. Solid–Liquid and Solid–Solid Phase Diagrams of Self-Assembled Triblock Janus Nanoparticles from Solution. *J. Phys. Chem. C* **2018**, *122*, 9235–9244, DOI: 10.1021/acs.jpcc.8b02043.

(38) Safaei, S.; Archereau, A. Y. M.; Hendy, S. C.; Willmott, G. R. Molecular dynamics simulations of Janus nanoparticles in a fluid flow. *Soft Matter* **2019**, *15*, 6742–6752, DOI: 10.1039/C9SM00694J.

(39) Safaei, S.; Todd, C.; Yarndley, J.; Hendy, S. C.; Willmott, G. R. Asymmetric assembly of Lennard-Jones Janus dimers. *Phys. Rev. E* **2021**, *104*, 024602, DOI: 10.1103/PhysRevE.104.024602.

(40) Bahri, K.; Eslami, H.; Müaller-Plathe, F. Self-Assembly of Model Triblock Janus Colloidal Particles in Two Dimensions. *J. Chem. Theory Comput.* **2022**, *18*, 1870–1882, DOI: 10.1021/acs.jctc.1c01116.

(41) Casagrande, C.; Fabre, P.; Raphael, E.; Veyssie, M. Water/Oil Interfaces. *Europhys. Lett.* **1989**, *9*, 251–255, DOI: 10.1209/0295-5075/9/3/011.

(42) Cayre, O.; Paunov, V. N.; Velev, O. D. Fabrication of Asymmetrically Coated Colloid Particles by Microcontact Printing Techniques. *J. Mater. Chem.* **2003**, *13*, 2445–2450, DOI: 10.1039/B308817K.

(43) Cayre, O.; Paunov, V. N.; Velev, O. D. Fabrication of Dipolar Colloid Particles by Microcontact Printing. *Chem. Commun.* **2003**, *39*, 2296–2297, DOI: 10.1039/B307296G.

(44) Takahara, Y. K.; Ikeda, S.; Ishino, S.; Tachi, K.; Ikeue, K.; Sakata, T.; Hasegawa, T.; Mori, H.; Matsumura, M.; Ohtani, B. Asymmetrically Modified Silica Particles: A Simple Particulate Surfactant for Stabilization of Oil Droplets in Water. *J. Am. Chem. Soc.* **2005**, *127*, 6271–6275, DOI: 10.1021/ja043581r.

(45) Nur, H.; Ikeda, S.; Ohtani, B. Phase-Boundary Catalysis: A New Approach in Alkene Epoxidation with Hydrogen Peroxide by Zeolite Loaded with Alkylsilane-Covered Titanium Oxide. *Chem. Commun.* **2000**, *19*, 2235–2236, DOI: 10.1039/b006207n.

(46) Hong, L.; Jiang, S.; Granick, S. Simple Method to Produce Janus Colloidal Particles in Large Quantity. *Langmuir* **2006**, *22*, 9495–9499.

(47) Goyal, A.; Hall, C. K.; Velev, O. D. Self-Assembly in Binary Mixtures of Dipolar Colloids: Molecular Dynamics Simulations. *J. Chem. Phys.* **2010**, *133*, 064511, DOI: 10.1063/1.3477985.

(48) Bianchi, E.; Kahl, G.; Likos, C. N. Inverse patchy colloids: from microscopic description to mesoscopic coarse-graining. *Soft Matter* **2011**, *7*, 8313–8323, DOI: 10.1039/C1SM05597F.

(49) Stipsitz, M.; Kahl, G.; Bianchi, E. Generalized inverse patchy colloid model. *J. Chem. Phys.* **2015**, *143*, 114905, DOI: 10.1063/1.4930600.

(50) Labbe-Laurent, M.; Dietrich, S. Critical Casimir interactions between Janus particles. *Soft Matter* **2016**, *12*, 6621–6648, DOI: 10.1039/c6sm00990e.

(51) Bafi, N. F.; Nowakowski, P.; Dietrich, S. Effective pair interaction of patchy particles in critical fluids. *J. Chem. Phys.* **2020**, *152*, 114902, DOI: 10.1063/5.0001293.

(52) Jonas, H. J.; Stuij, S. G.; Schall, P.; Bolhuis, P. G. A temperature-dependent critical Casimir patchy particle model benchmarked onto experiment. *J. Chem. Phys.* **2021**, *155*, 034902, DOI: 10.1063/5.0055012.

(53) Derjaguin, B. Untersuchungen über die Reibung und Adhäsion, IV. *Kolloid-Zeitschrift* **1934**, *69*, 155–164, DOI: 10.1007/BF01433225.

(54) Derjaguin, B.; Landau, L. Theory of the Stability of Strongly Charged Lyophobic Sols and of the Adhesion of Strongly Charged Particles in Solutions of Electrolytes. *Acta Physicochim. U.R.S.S.* **1941**, *14*, 633.

(55) Derjaguin, B.; Landau, L. Theory of the Stability of Strongly Charged Lyophobic Sols and of the Adhesion of Strongly Charged Particles in Solutions of Electrolytes. *Prog. Surf. Sci.* **1993**, *43*, 30–59, DOI: 10.1016/0079-6816(93)90013-L.

(56) Verwey, E. J. W.; Overbeek, J. T. G. *Theory of the Stability of Lyophobic Colloids*; Elsevier: Amsterdam, 1948; p 205.

(57) Ohshima, H. *Biophysical Chemistry of Biointerfaces*; John Wiley & Sons, Ltd, 2010; DOI: 10.1002/9780470630631.

(58) Weeks, J. D.; Chandler, D.; Andersen, H. C. Role of Repulsive Forces in Determining the Equilibrium Structure of Simple Liquids. *J. Chem. Phys.* **1971**, *54*, 5237, DOI: 10.1063/1.1674820.

(59) Chen, Q.; Whitmer, J. K.; Jiang, S.; Bae, S. C.; Luijten, E.; Granick, S. Supracolloidal Reaction Kinetics of Janus Spheres. *Science* **2011**, *331*, 199–202, DOI: 10.1126/science.1197451.

(60) Chen, Q.; Diesel, E.; Whitmer, J. K.; Bae, S. C.; Luijten, E.; Granick, S. Triblock Colloids for Directed Self-Assembly. *J. Am. Chem. Soc.* **2011**, *133*, 7725–7727, DOI: 10.1021/ja202360g.

(61) Bhattacharjee, S.; Elimelech, M.; Borkovec, M. DLVO Interaction between Colloidal Particles: Beyond Derjaguin's Approximation. *Croat. Chem. Acta* **1998**, *71*, 883–903.

TOC Graphic